

# Changes in the North Sea Extreme Waves

SOFIA CAIRES<sup>1</sup> and JACCO GROENWEG  
WL | Delft Hydraulics, Delft, Netherlands

ANDREAS STERL  
Royal Netherlands Meteorological Institute, De Bilt, Netherlands

## 1. Introduction

The current approach to obtain hydraulic boundary conditions for the Dutch water defences involves the transformation of offshore wave conditions to nearshore. The transformation consist of defining uniform wind fields with extreme wind velocities and associated offshore wave conditions, and using these to run the wave model SWAN (Simulation of Waves in Nearshore Areas, Ris et al., 1999) in stationary mode, computing the corresponding nearshore extreme waves. There are two aspects in this approach that may have a negative effect on the quality of nearshore extreme value estimates. First, the stationary assumption may not hold, either the modelled storm never occurs or occurs with a different return period. Secondly, in the current approach no attention is paid to effects of climate variability on wave extremes.

In this study, we use SWAN in the non-stationary mode to produce a timeseries of nearshore long-term wave heights and analyse it using both stationary and a non-stationary extreme value models. Our final goal is to answer questions such as: What are the differences between the extreme value estimates obtained using a non-stationary wave modelling approach and those obtained with the currently used stationary approach? Has the North Sea extreme wave climate changed in the last decades, and how is it expected to change in the future?

In terms of future changes in wave climate, this is essentially an illustrative study indicating how one can obtain preliminary estimates of possible effects of climate change in the definition of hydraulic boundary conditions for the Dutch coast.

More specifically, the area that we consider in this study is the coastal strip in front of the Dutch Petten sea defence. In this area, the Dutch Ministry of Public Works maintains a network of buoys aligned approximately perpendicularly to the Petten coast line. The measuring location furthest from the shore is the MP1 location

which is at a distance of about 8 km from the coast and at 20-m depth. ERA-40 data is used and provides wind fields and wave boundary conditions for the SWAN hindcast. A SWAN model setup is defined in order to hindcast waves at MP1. The defined model is then calibrated based on hindcasts of two characteristic storms for which measurements from the waverider at MP1 are available.

Using the calibrated model, wave hindcasts from 1958 to 2001 at MP1 are computed.

The hindcast timeseries of significant wave height ( $H_s$ ) at MP1 is analysed using a stationary extreme value approach. The 100-yr return value estimate obtained from such analysis is then compared with the corresponding estimate obtained by running SWAN in stationary mode with the estimated 100-yr uniform wind field and the corresponding wave boundary conditions.

In order to look for trends or other systematic temporal variations of  $H_s$  in the last decades at MP1, the hindcast timeseries is also analyzed using a non-stationary extreme value approach.

## 2. The SWAN model

### 2.1 Model description

The SWAN model is freely available and was developed at Delft University of Technology. A detailed description of the model as it was initially developed can be found in Ris et al. (1999) and a description of the latest version in Booij et al. (2004).

The model solves the action balance equation, in Cartesian or spherical coordinates, without any ad hoc assumption on the shape of the wave spectrum. In Cartesian coordinates the equation is

$$\frac{\partial N}{\partial t} + \frac{\partial}{\partial x}(c_x N) + \frac{\partial}{\partial y}(c_y N) + \frac{\partial}{\partial \sigma}(c_\sigma N) + \frac{\partial}{\partial \theta}(c_\theta N) = \frac{S_{tot}}{\sigma}, \quad (2.1)$$

where  $N$  is the action density,  $t$  is the time,  $\sigma$  is the

---

1 Corresponding author: P.O. Box 177, 2600 MH Delft, Netherlands. Email: sofia.caires@wldelft.nl

relative angular frequency, and  $\theta$  the wave direction.

The first term on the left-hand side of Eq. (2.1) represents the local rate of change of action density in time. The second and third terms represent propagation of action in geographical space. The fourth term represents shifting of the relative frequency due to variation in depth and currents. The fifth term represents depth-induced and current-induced refractions. The quantities  $c_x$ ,  $c_y$ ,  $c_\theta$  and  $c_\sigma$  are the propagation speeds in the geographical x- and y-space, and in the  $\theta$ - and the  $\sigma$ -space, respectively. The expressions of these propagation speeds are taken from linear wave theory.

In (2.1)  $S_{tot}$  is the energy source term. This source term is the sum of separate source terms representing different types of processes: wave energy growth by wind input, wave energy transfer due to non-linear wave-wave interactions (both quadruplets and triads), and the decay of wave energy due to whitecapping, bottom friction, and depth induced wave breaking.

For some source terms more than one formulation is implemented in SWAN. We will not give the expression of all these terms (see Booij et al. (2004)), but only of those which are relevant to our discussion.

The wind input source term is given by the sum of a linear and an exponential term. The linear term represents Philips' resonance mechanism and is given by the expression of Cavaleri and Malanotte-Rizzoli (1981),

$$S_{w,lin} = \frac{\alpha}{2\pi g^2} \exp\left[-\left(\frac{\sigma}{\sigma_{PM}}\right)^4\right] (U_* \max(0, \cos(\theta - \theta_*)))^4, \quad (2.2)$$

where  $\alpha$  is the proportionality coefficient,  $g$  is the acceleration of gravity, the subscript PM denotes the value of the variable for fully developed sea states according to Pierson and Moskowitz (1964), and  $U_*$  is the wind friction velocity. The exponential term accounts for Miles' feedback mechanism. In SWAN the expressions of Komen et al. (1984) and Janssen (1991) have been implemented. The former is a function of the friction velocity divided by the phase speed of the waves ( $U_*/c_{ph}$ ), and the latter of  $(U_*/c_{ph})^2$ .

In deep water, quadruplet wave interactions dominate the evolution of the spectrum. These nonlinear wave-wave interactions transfer energy from the peak frequency to lower frequencies (moving the peak to lower frequencies) and to higher frequencies (where it is dissipated by whitecapping). The expression of the quadruplet source term can be obtained theoretically without using poor fundamental hypotheses or approximations. However, its full computation is extremely time consuming. Therefore, a discrete operator introduced by Hasselmann and Hasselmann (1985) is also available in SWAN to take

into account the quadruplet non-linear energy transfer.

In very shallow water triad wave interaction transfer energy at two frequency components to both the sum-frequency, resulting in higher harmonics, and the difference frequency, resulting in lower harmonics. In SWAN this phenomenon is taken into account only with respect to the generation of higher harmonics by means of the lumped triad approximation of Eldeberky (1996).

The wave dissipation term is still the less known in the wave balance equation. SWAN's formulation of dissipation by whitecapping is based on the pulse-based model of Hasselmann (1974), as adapted by the WAMDI group (1988):

$$S_{ds}(\sigma, \theta) = -\Gamma \bar{\sigma} \frac{k}{k} E(\sigma, \theta), \quad (2.3)$$

where

$$\Gamma = C_{ds} \left( (1 - \delta) + \delta \frac{k}{k} \right) \left( \frac{\bar{s}}{\bar{s}_{PM}} \right)^4, \quad (2.4)$$

a bar over a variable denotes its mean,  $k$  is the wavenumber, and  $s$  the wave steepness. The remaining parameters in  $\Gamma$  depend on the wind input formulation that is used and are determined by closing the energy balance of the waves in fully developed conditions. For situations for which the exponential wind growth expression of Komen et al. (1984) is used,  $C_{ds} = 2.36 \cdot 10^{-5}$  and  $\delta = 0$ , and when the formulation of Janssen (1991) is used  $C_{ds} = 4.10 \cdot 10^{-5}$  and  $\delta = 0.5$ .

We shall refer to the use of the exponential wind growth expression of Komen et al. (1984) and the corresponding whitecapping formulations as a *WAM3 configuration*, and to the use of the exponential wind growth expression of Janssen (1991) and the corresponding whitecapping formulations as a *WAM4 configuration* (see Komen et al., 1994).

As to SWAN's numerical approach, the integration of the propagation and of the source terms of Eq. (2.1) has been implemented with finite difference schemes in all four dimensions (geographical space and spectral space). A constant time increment is used for the time integration.

The model propagates the wave action density of all components of the spectrum across the computational area using implicit schemes in geographical and spectral space, supplemented with a central approximation in spectral space. In geographical space the scheme is upwind and applied to each of the four directional quadrants of wave propagation in sequence. Three of such schemes are available in SWAN: a first-order backward space, backward time (BSBT) scheme, a second-order upwind scheme with second order diffusion (the SORDUP scheme) and a second order upwind

scheme with third order diffusion (the S&L scheme). The numerical schemes used for the source term integration are essentially implicit.

In order to match physical scales at relatively high frequencies and to ensure numerical stability at relatively large time steps, a limiter (Ris, 1997) controlling the maximum total change of action density per iteration at each discrete wave component is imposed.

## 2.2 Studies and extensions

As can be seen from the above description, SWAN is quite a versatile program in which different numerical schemes and physics can be chosen. In order to facilitate its initial use, default settings have been defined and should provide a good first choice in most applications (see Booij et al., 2004). The model can therefore be implemented using the default settings, i.e. without taking the available choices into consideration. Several calibration studies have aimed to optimise SWAN's results by changing its default settings. Most of the published studies focus on the stationary version of SWAN, and only a few consider the performance of the non-stationary mode.

Motivated by deficiencies in the SWAN hindcast of the SandyDuck '97 experiment (Rogers et al., 2000), namely the underprediction of low and medium frequency energy in the wind sea portion of the spectrum (.12-.19 Hz) and the dissipation of swell (.05-.12 Hz) due to the presence of wind sea, Rogers et al. (2003) investigate the physics used in the SWAN wave model. Because the whitecapping term is the less accurate of the deep water source function terms, Rogers et al. (2003) focus their attention on that term.

Following Komen et al. (1994, p.145) they rewrite Eq. (2.3) in the form

$$S_{ds}(\sigma, \theta) = C_{ds} \left( \frac{\bar{s}}{\bar{s}_{PM}} \right)^4 \bar{\sigma} \left( \frac{k}{\bar{k}} \right)^n E(\sigma, \theta) \quad (2.5)$$

For  $n = 1$  the right-hand side of (2.5) is proportional to  $k/\bar{k}$ , as in SWAN's default whitecapping formulation that is used in combination with the exponential wind growth expression of Komen et al. (1984). Increasing the parameter  $n$  above 1 has the effect of reducing dissipation at lower frequencies while increasing dissipation at higher frequencies. With  $n=1.5$  the dependence of  $S_{ds}$  on  $k/\bar{k}$  is close to that in SWAN's default whitecapping formulation used in combination exponential wind growth expression of Janssen (1991).

Rogers et al. (2003) looked for effective ways of reducing

dissipation of lower frequency energy in SWAN by changing the parameters of the dissipation term present in Eq. (2.5). In all their computations the exponential wind growth expression of Komen et al. (1984) was used and their results showed that increasing  $n$  in (2.5) up to 2 lead to improvements in hindcasts as long as  $C_{ds}$  was defined so that for fetch unlimited and duration unlimited conditions the total energy levels are similar to those of the default SWAN setting. However, Rogers et al. (2003) vent criticisms on the tuning of the dissipation terms made in order that the bulk parameters match empirically based quasi-equilibrium target values at the model infinite-duration and -fetch asymptote. They argue that, in a temporal sense, the asymptotes of these models may be well tuned, but the accuracy of the rate at which the models approach these asymptotes is uncertain. They conclude that the problem of wind sea having an illogical and physically unjustified impact on swell must be addressed using a totally new approach.

Toulany et al. (2002) use SWAN in non-stationary mode to hindcast storms in the Canadian northwest Atlantic coast. They have looked at the differences between the results obtained when using the WAM3 or the WAM4 configurations, and report that for 20 m/s winds using WAM3 configuration always results in  $H_s$  hindcasts higher than those obtained using WAM4 configuration. The results obtained based on WAM3 comparing better with measurements. For long duration (>24hr) and large fetch sea states, the differences can be as much as 50% in locations with depths in excess of 50 m. However, as the depths decrease the  $H_s$  estimates obtained using the WAM3 and the WAM4 configuration converge to each other.

Problems in SWAN's WAM4 configuration have been reported by Booij et al. (1999), for which reason the exponential wind growth expression of Janssen (1991) was not considered in the study of Rogers et al. (2003).

Yin et al. (2005) use SWAN for hindcasts storms in the Bohai Sea. They run SWAN using the WAM3 and the WAM 4 configurations, and observe that each of the hindcasts underestimates the wave height at the peak of the storms. The results of computations using the WAM4 configuration were as much as 2 m lower than those obtained using the WAM3 configuration.

In order to improve their hindcasts they have substituted the proportionality coefficient of Eq. (2.2) by a variable depending on  $U_*$  for moderate wind speeds and which may yield values of  $\alpha$  as high as 0.15 (100 times SWAN's default value, which is  $\alpha = 0.0015$  as suggested by Cavaleri and Malanotte-Rizzoli, 1981). Their hindcasts using the  $U_*$  dependent proportionality coefficient compared quite well to the available

measurements irrespective of the configuration (WAM3 or WAM4) being used.

Lalbeharry et al. (2004) ran SWAN using the WAM3 and the WAM4 configurations to hindcast three weeks of observations in the Canadian Lake Erie. The SWAN hindcasts using the WAM3 configuration compare reasonably well with the observations, but the hindcast using the WAM4 configuration are poorer. The latter, although reproducing better the peak period measurements, severely underestimates the storms  $H_s$ .

Lalbeharry et al. (2004) argue that the exponential wind growth of Janssen (1991) is not properly implemented in SWAN. They remove the implemented shift growth parameter and activate the limiter of Hersbach and Janssen (1999) instead of the limiter of Ris (1997) when using SWAN's WAM4 configuration and show that the peak period hindcasts remain superior and that the new  $H_s$  results are similar to those obtained using the WAM3 configuration.

It should be noted that, although SWAN's default wind input and whitecapping configuration is WAM3, SWAN's manual contains no word of caution about using the available WAM4 formulation.

Van der Westhuysen et al. (2005) report that when using SWAN's WAM3 configuration to hindcast pure wind sea, the energy density at lower frequencies is typically underpredicted, whereas energy levels in the high-frequency tail are generally overpredicted. When hindcasting a combined swell-sea situation, SWAN predicts more dissipation of swell in the presence of wind sea than in its absence, and a reduced dissipation of wind sea in the presence of swell, leading to accelerated wave growth.

In order to improve SWAN's hindcasts they propose using a whitecapping dissipation source term based on Alves and Banner (2003) with no dependence on spectral mean quantities, and an wind input source term based on that of Yan (1987) which depends on both  $(U_*/c_{ph})$  and  $(U_*/c_{ph})^2$ . In order to obtain a  $f^{-4}$  high frequency spectral tail they build a dependence of the whitecapping source term on wave age. The resulting combination of wind input and whitecapping source terms was calibrated against fetch- and depth-limited growth curves.

The results of the SWAN computations using the new formulation, which we shall refer to as the Westh. configuration, were compared with those of computations using the WAM3 configuration in three field cases. The results based on both configurations compared rather well with the observations, but results based on the Westh. configuration compared better. The results based on the WAM3 configuration had a high frequency tail

heavier than the measured one, which the new formulation results reproduced quite accurately.

The just released SWAN version 40.51 has the Westh. configuration available.

### 3. The ERA-40 data

In 2003 the European Centre for Medium Range Weather Forecasts (ECMWF) completed ERA-40, a global atmospheric reanalysis covering the period from September 1957 to August 2002. This reanalysis was carried out using ECMWF's Integrated Forecasting System, a coupled atmosphere-wave model with variational data assimilation. This is a state-of-the-art model and is very similar to the one used operationally for weather forecasts, though with lower resolution. The aim of the reanalysis was to produce a dataset with no inhomogeneities as far as the technique of analysis is concerned, by reconstructing decades of data using the same numerical model throughout. A distinguishing feature of ECMWF's model is its coupling to a deep water wave model, the well-known WAM (Komen et al., 1994), through the wave height dependent Charnock parameter (see Janssen et al., 2002). This makes wave data a natural output of ERA-40.



Figure 3.1 Aerial view of the Petten region. Red crosses indicate the location of the ERA-40 gridpoints. The location of the offshore K13 and YM6 buoys and the nearshore MP1 buoy are flagged.

The ERA-40 data set, which is freely available for scientific purposes, includes 6-hourly global fields of wind speed at 10 meters height ( $U_{10}$ ) and wave parameters, such as  $H_s$ , mean zero-upcrossing wave period ( $T_{m02}$ ) and mean wave direction (MWD) on a global  $1.5^\circ \times 1.5^\circ$  latitude/longitude grid.

Figure 3.1 shows the locations of the ERA-40 gridpoints

surrounding the Petten region, the nearshore Petten buoy (MP1) and the offshore buoys maintained by Dutch Ministry of Public Works, the K13 and the YM6 buoys.

#### 4. Model setup and calibration

With the goal of calibrating the non-stationary version of SWAN for our application we have hindcast two storms in the North Coast of the Netherlands for which measurements from the directional waverider located at MP1 are available.

The hindcasts were carried out with SWAN version 40.51.

##### 4.1 Grids

The geographical domain used for the SWAN modeling extends from the coast of The Netherlands to the ERA-40 gridpoints surrounding the region of interest. A regular computational grid with a resolution of 1 km by 1 km was defined. Figure 4.1 shows the region covered by the SWAN grid and the corresponding bathymetry. The grid on which the bathymetry is given coincides with the computational grid.

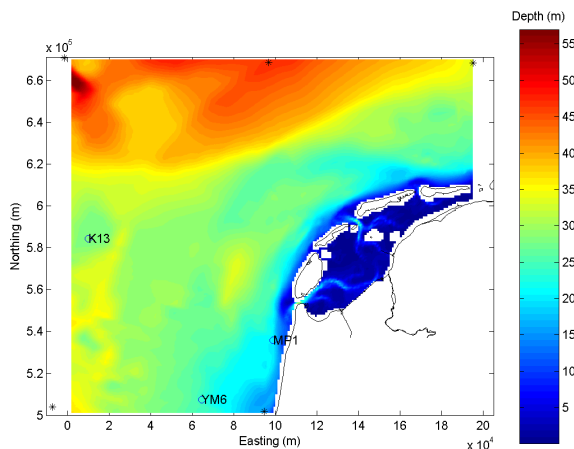


Figure 4.1 Region covered by the SWAN grid and the associated bathymetry. The asterisks indicate the ERA-40 gridpoints locations.

In terms of spectral resolution, a directional resolution of 10 degrees is used and the spectra are discretized in 37 frequencies distributed logarithmically between 0.03 and 1 Hz.

##### 4.2 Model settings

For our reference run we have used the default settings of SWAN with triads activated and the BSBT numerical

scheme (instead of the S&L scheme which is the SWAN default for non-stationary runs). A spin-up of at least 2 days was used in each storm hindcast. The integration time step was set to 20 minutes. 6-hourly ERA-40 waves and winds were given as input. No currents were incorporated and the water level was set to zero.

##### 4.3 Boundary wave conditions

The ERA-40 6-hourly wave data were applied at their respective locations at the boundaries of the SWAN grid (cf. the 5 red crosses in Figure 3.1 and the corresponding asterisks in Figure 4.1). These boundary conditions were given parametrically, and the wave parameters used were the  $H_s$ ,  $T_{m02}$  (converted to  $T_{m01}$  using the JONSWAP relations; Hasselmann et al., 1973) and MWD from ERA-40. A directional spreading (DSpr) of  $30^\circ$  was assumed.

In SWAN's east, south and north boundaries the data are linearly interpolated from one boundary location to the next. E.g. in the Eastern boundary the data is the linear interpolation between the defined conditions in the northern edge (using data from the ERA-40 gridpoint located at  $3^\circ\text{E}$ ,  $54.5^\circ\text{N}$ ) and those defined in the southern edge of the boundary (using data from the ERA-40 gridpoint located at  $3^\circ\text{E}$ ,  $52^\circ\text{N}$ ). The defined conditions in the northwestern edge of SWAN's grid (using data from the ERA-40 gridpoint located at  $6^\circ\text{E}$ ,  $54.5^\circ\text{N}$ ) are applied uniformly in SWAN's open western boundary (from the Wadden Sea to the edge with the Northern boundary; see Figure 4.1).

##### 4.4 Wind input

The ERA-40 wind fields are given on a regular grid covering the SWAN grid and with the gridpoints locations coinciding with the ERA-40 gridpoint locations. The grid resolution is of 97.5 km in the West-East direction and of 170 km in the South-North direction. The data are given every 6 hours. SWAN will interpolate the data to the SWAN grid.

##### 4.5 Calibration

Two storms for which measurements are available in the MP1 location have been considered in this study. The first storm occurred from 3 to 6 February 1999 and reached its observed peak at MP1 on the 5<sup>th</sup> of February at 12:00h; we shall refer to it as the *1999 storm*. The second storm to be considered is the *1995 storm*, which occurred from 1 to 2 January 1995 and reached its

observed peak at MP1 on the 2<sup>th</sup> of January at 6:00h.

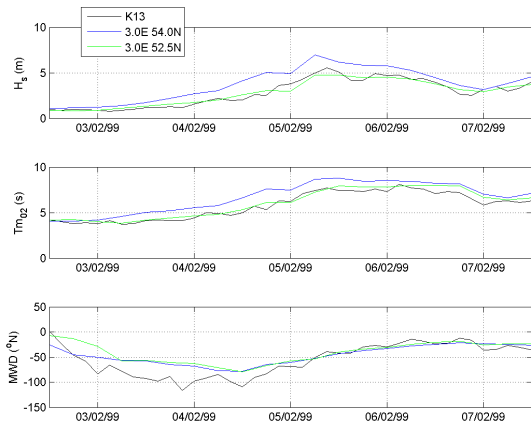


Figure 4.2 Timeseries of the wave measurements at K13 and the corresponding ERA-40 data at the nearby gridpoints during the 1999 storm.

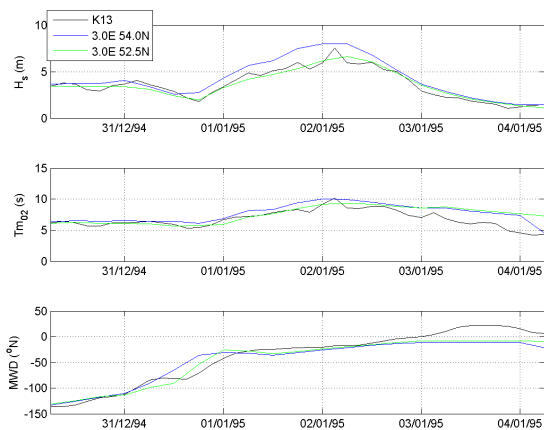


Figure 4.3 Timeseries of the wave measurements at K13 and the corresponding ERA-40 data at the nearby gridpoints during the 1995 storm.

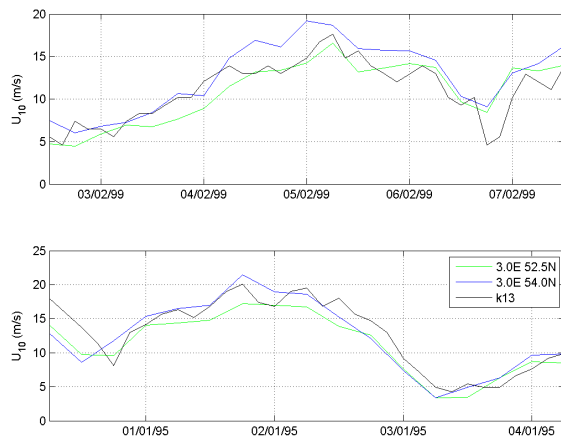


Figure 4.4 Timeseries of the wind speed measurements at K13 and the corresponding ERA-40 data at the nearby gridpoints.

Figures 4.2 and 4.3 compare the offshore wave

measurements at the K13 locations and the ERA-40 data at the nearby gridpoints during the 1999 storm and the 1995 storm, respectively.

In general the ERA-40 data compares well to the measurements, apart from some overestimation of  $H_s$  and  $T_{m02}$ . For the mean wave direction (MWD) the correspondence between ERA-40 and the measurements is rather poor in the initial period of the 1999 storm.

Figure 4.4 compares the wind velocity measured at the K13 location with the corresponding ERA-40 data at nearby gridpoints in both storms. There is some underestimation of the wind velocity in the initial period of the 1999 storm, but generally the data compares rather well with the measurements.

In order to find the optimal parameters and boundary conditions for the hindcast of waves in the MP1 location we have ran SWAN using different settings and compared the hindcast of the 1999 storm with the measurements. Once the best settings for hindcasting the 1999 storm are established, we validate the settings for the 1995 storm. Our default hindcasts are carried out using

- the WAM3 configuration, the BSBT numerical scheme with a 20 minutes integration time step, and the SWAN default values for the remaining model settings;
- the ERA-40 boundary wave data as described in Section 4.3;
- the ERA-40 input wind fields as described in Section 4.4; and
- water level equal to zero and no current fields.

The MP1 measurements are available hourly and there is a large amount of sampling variability in the data (see the dotted black line in Figure 4.5). This is absent in the hindcasts given that the ERA-40 boundary data is available only every 6 hours and with a  $1.5^\circ \times 1.5^\circ$  spatial resolution. In order to remove some of the sampling variability from the measurements, 3-hourly averages were computed (see the full black line in Figure 4.5).

In order to study the sensitivity of the results to the time step and to the numerical scheme we have performed several hindcasts of the 1999 storm using different integration schemes and time steps.

Figure 4.5 shows  $H_s$  measurements at MP1 and the corresponding SWAN hindcast using the BSBT and the S&L numerical scheme with a time step of 7.5 minutes (the maximum time step allowed for these computations by the S&L scheme) and the BSBT numerical scheme with larger time steps. The  $H_s$  hindcasts, although

showing the same time variation as the measurements, underestimate the high  $H_s$  measurements. However, the quality of the hindcasts does not depend on the time scheme nor on the integration time step used. A time step of 1 hour in combination with the BSBT numerical scheme produces results similar to those obtained with the smaller time steps and a more advanced numerical scheme.

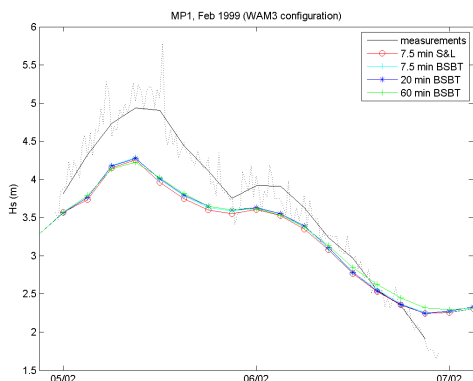


Figure 4.5 MP1 measurements of the 1999 storm (black lines) and SWAN hindcast using different numerical schemes and integration time steps.

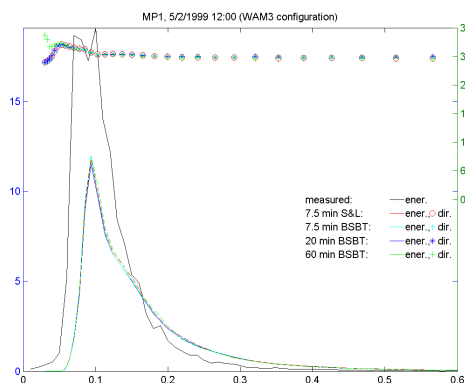


Figure 4.6 MP1 3-hourly averaged frequency spectra for 5/2/1999 12:00 (black lines) and the corresponding SWAN spectra and frequency dependent MWD computed using different numerical schemes and integration time steps.

Figure 4.6 shows the 3-hourly averaged wave spectra measured at MP1 around 12:00 of the 5<sup>th</sup> of February 1999 and the corresponding SWAN spectra from the different runs, mentioned above. Again, it can be seen that the SWAN hindcasts underestimate the significant wave height. The underestimation is caused by underestimation of the wave energy at frequencies lower than 0.18 Hz, which indicates that the mean wave period is also severely underestimated. In fact, in all time instances of the storm SWAN underestimates  $T_{m01}$  by approximately 2 seconds (figure not shown). Also, in terms of the frequency spectra the quality of the hindcasts does not depend on the time scheme nor on the

integration time step used.

In order to study the sensitivity of the results to the choice of the combination of wind growth and whitecapping dissipation formulations, we have performed hindcasts of the 1999 storm using the WAM3, WAM4 and Westh. configurations. The results are compared in Figures 4.7 and 4.8.

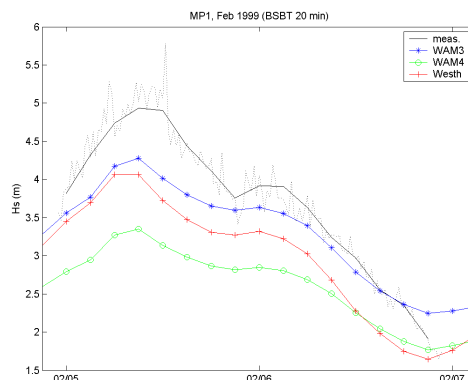


Figure 4.7 MP1 measurements of the 1999 storm (black lines) and SWAN hindcasts using the WAM3 (blue line), the WAM4 (green line) and the Westh (red line) configurations.

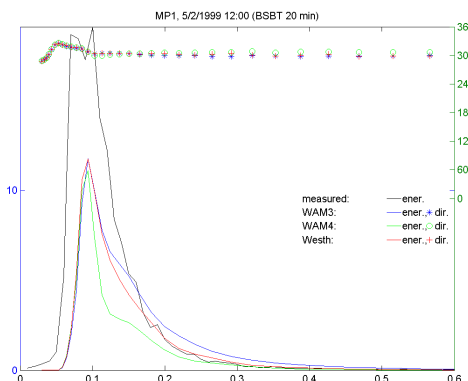


Figure 4.8 MP1 3-hourly averaged frequency spectra for 5/2/1999 12:00 and the corresponding SWAN spectra and frequency dependent MWD computed using the WAM3, the WAM4 and the Westh configurations.

In terms of the significant wave height, all hindcasts underestimate the measurements, the hindcasts using the WAM3 configuration getting closest to the measurements. In terms of spectral form, the hindcasts using the Westh configuration are those which compare better with the measurements, reproducing the measured high frequency tail rather well. The underestimation of the mean wave periods is also smaller for the hindcasts using the Westh. configuration (not shown). With the objective of bringing the hindcasts closer to the measurements we have looked for the most effective changes in the SWAN settings and boundary conditions. We have considered a total of 5 deviations from our default hindcast configuration:

- At the offshore boundaries a directional spreading of  $30^\circ$  is imposed; however, in long period sea states observed values for the directional spreading are often lower than  $30^\circ$ . We have therefore produced hindcasts fixing the value at  $15^\circ$ .
- There is some evidence of a small underestimation of the wind speed by the ERA-40 data. Also, not accounting for sub-grid scale variability (both in space and time) in the ERA-40 winds may result in too low significant wave height hindcasts. To compensate for this, we have produced hindcasts using a 10% higher ERA-40 input wind field.
- Following the suggestion of Yin et al. (2005), we have activated the linear wind growth term with a proportionality coefficient of 0.003 (twice the default value) and 0.10 (the value used by Yin et al. (2005) for wind speed of about 10 m/s).
- We have produced hindcasts using a spatially and temporally constant water level of 2 m to account for an eventual storm surge.

The resulting hindcasts are compared in Figure 4.9.

All the deviations considered lead to the desired increase of the significant wave height:

- The hindcasts based on a lower value of the directional spreading show less underestimation of the significant wave height at the peak of the storm and differ only slightly from the default hindcast at other instances. These comparisons thus suggest that the imposed value for the directional spreading at the boundaries in the default hindcast is too high.
- The hindcasts based on a 10% higher wind speed field compare reasonably well with the measurements. Although this may not be due to underestimation of the wind speed by ERA-40 data, but more due to sub-grid scale variability not being taken into account or other factors, such increase of the wind speeds is effective in improving the results.
- The activation of the linear wind growth term with a proportionality coefficient of 0.003 lead to a hindcast differing only slightly from the default hindcast. The results based on a proportionality coefficient of 0.1, although having higher values for the significant wave height in the growing stage of the storm, produce spectral forms that compare rather poorly with the measurements. Based on these results we see no reason to activate SWAN's linear wind growth term.
- Changing the water level from 0 m to 2 m lead to and increase of approximately 20 cm in significant wave height. There is however no reason to assume

that such water level would be maintained in the whole period. Since the changes in the results are rather small we find that the best is to maintain a zero water level.

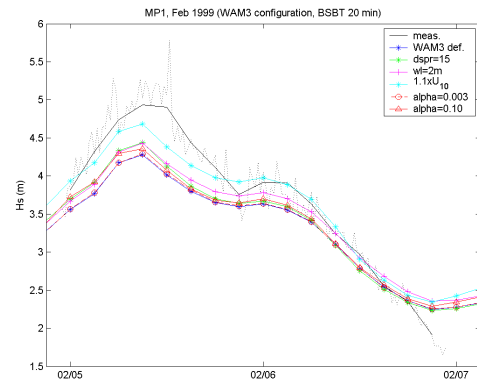


Figure 4.9 MP1 measurements of the 1999 storm (black lines) and SWAN hindcasts using different setting and boundary and input conditions.

Based on our sensitivity study described above, we have decided that the directional spreading of the waves at the offshore boundary should be set at  $20^\circ$  and that the input wind fields should be increased by 10%.

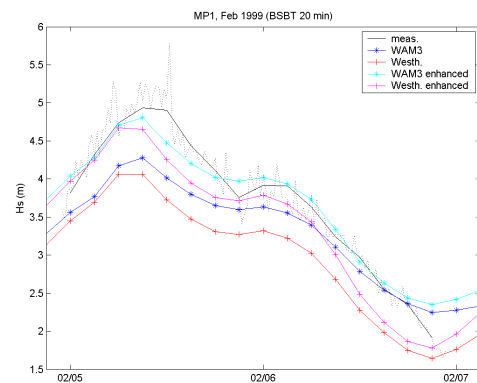


Figure 4.10 MP1 measurements of the 1999 storm (black lines) and SWAN hindcasts based on the WAM3 (blue line), the Westh (red line), the enhanced WAM3 (light blue line), and the enhanced Westh (pink line) configurations.

Using the calibrated input and boundary conditions we have produced new SWAN hindcast of the 1999 based on the WAM3 and Westh. configuration. We refer to the results based on the calibrated boundary and input conditions as *enhanced*. The results are compared in Figure 4.10. Although the hindcasts based on the enhanced Westh. configuration describe the high frequency tail of the measured spectra and the measured mean wave periods better (figure not shown), the correspondence between the hindcasts based on the enhanced WAM3 configuration and the significant wave height measurements is superior. The results based on the Westh. configuration overestimate the decay of wave

energy following the storm peak.

Using calibrated input and boundary conditions (a directional spreading of  $20^\circ$  and input wind fields increased by 10%) we have produced SWAN hindcast of the 1995 storm as well, based on the WAM3 and Westh. configuration. The results are compared with the measurements in Figure 4.11.

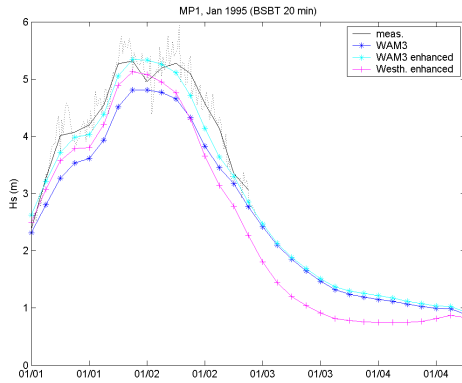


Figure 4.11 MPI measurements of the 1995 storm (black lines) and SWAN hindcasts based on the WAM3 (blue line), the enhanced WAM3 (light blue line), and the enhanced Westh (pink line) configurations.

The hindcast based on the WAM3 configuration and the enhanced boundary and input conditions are those that compare better with the significant wave height measurements. Again, although the hindcasts based on the enhanced Westh. configuration describe the high frequency tail of the measured spectra and the measured mean wave periods better (figures not shown), the results based on the Westh. configuration overestimate the decay of wave energy following the storm peak.

## 5 Extreme values

### 5.1 Theory

One of the currently most used methods in extreme value analyses in the stationary setting is the peaks-over-threshold (POT) method, in which the occurrence of ‘storms’ above a certain threshold and the magnitude of peak observations from ‘independent’ storms are modeled with Poisson and Generalized Pareto (GPD) distributions, respectively (see e.g. Coles, 2001, or Caires and Sterl, 2005).

More precisely, in the POT method, the peak excesses over a high threshold  $u$  of a timeseries are assumed to occur according to a Poisson process with rate  $\lambda_u$  and to be independently distributed with a GPD, whose distribution function is given by

$$F_u(x) = 1 - (1 + \xi x / \sigma)^{-1/\xi},$$

where  $0 < x < \infty$ ,  $\sigma > 0$  and  $-\infty < \xi < \infty$ . The two parameters of the GPD are called the *scale* ( $\sigma$ ) and *shape* ( $\xi$ ) parameters. For  $\xi = 0$  the GPD is the exponential distribution with mean  $\sigma$ , for  $\xi > 0$  it is the Pareto distribution, and for  $\xi < 0$  it is a special case of the beta distribution. The GPD is said to have a type II tail for  $\xi > 0$  and a type III tail for  $\xi < 0$ . The tail of the exponential distribution is a type I tail.

In choosing the threshold there is a trade off between bias and variance: Too low a threshold is likely to violate the asymptotic basis of the model, leading to bias; too high a threshold will generate fewer excesses with which to estimate the model, leading to high variance. An important property of the POT/GPD approach is the threshold stability property: if a GPD  $F_{u_1}$  is a reasonable model for excesses of a threshold  $u_1$ , then for a higher threshold  $u_2$  a GPD  $F_{u_2}$  should also apply; the two GPD’s have identical shape parameter and their scale parameters are related by  $\sigma_2 = \sigma_1 + \xi(u_2 - u_1)$ . This property of the GPD can be used to find the minimum threshold for which a GPD model applies to the data.

The non-stationary analogue of the POT/GPD approach is the non-homogeneous Poisson process (NPP). In the point process approach to modelling extreme values (see Smith (1989), Anderson et al. (2001) and Coles (2001) for details), one looks at the times at which ‘high values’ occur and at their magnitude. If  $t$  denotes the generic time at which a high value occurs and if  $x$  is the corresponding magnitude of the variable of interest, then the point process consists of a collection of points  $(t, x)$  in a region of the positive quadrant of the plane. In practice, such a collection of points has first to be extracted from the original timeseries in such a way that the  $x$  components can be modeled as independent random variables. The way this is usually done with wave and similar data is by a process of ‘declustering’ in which only the peak exceedances (highest observations) in clusters of successive exceedances (‘storms’) of a specified threshold or level are retained and, of these, only those which in some sense are sufficiently apart (so that they belong to more or less ‘independent storms’) will be considered as belonging to the collection of points of the point process. The process of declustering is thus based on fixing a threshold over which one can consider exceedances and hence define the cluster peaks.

Thus our point process, or rather its ‘realization’, consists of a collection of points belonging to the plane set  $C = \{(t, x) : x > u, 0 \leq t \leq T\}$  where  $T$  is the number of years (in our case) over which observations are

available and  $u$  denotes the threshold at time  $t$ . The non-homogeneous Poisson process (NPP) model of extremes is specified by the following two properties. Firstly, if  $A$  is a subset of  $C$ , then the number of points occurring in  $A$ , which we denote by  $N(A)$ , is a random variable with a Poisson probability function with mean  $\rho(A)$ , where, writing  $x_+ = \max(0, x)$  for real  $x$ ,

$$\rho(A) = \int_A \lambda(t, x) dt dx,$$

$$\lambda(t, x) = \frac{1}{\sigma(t)} \left( 1 + \xi(t) \frac{x - \mu(t)}{\sigma(t)} \right)_+^{-\frac{1}{\xi(t)}} \text{ for } (t, x) \in C,$$

and  $\mu(t)$ ,  $\sigma(t)$  and  $\xi(t)$  are respectively the *location, scale and shape parameters* - or rather "parameter functions" - that may depend on time and need to be specified and estimated in practice.

The  $m$ -year return value,  $x_m$ , is determined by solving

$$\int_0^m \left( 1 + \xi(t) \frac{x_m - \mu(t)}{\sigma(t)} \right)_+^{-\frac{1}{\xi(t)}} dt = 1.$$

In order to incorporate non-stationarity into the process we shall consider the following models for its parameters:

$$\begin{aligned} \mu(t) &= \mu_0 + \mu_1 P(t) + \mu_2 G(t), \\ \sigma(t) &= \sigma_0 + \sigma_1 P(t) + \sigma_2 G(t) \text{ and } \xi(t) = \xi, \end{aligned} \quad (5.1)$$

$t=1, 2, \dots, T$ , where  $\mu_1$ ,  $\mu_2$ , etc., are constants and  $P(t)$  and  $G(t)$  are covariates, i.e., observations from a timeseries which for each time  $t$  are to a certain degree related to the peak  $x$  occurring at  $t$ .

The parameters of the NPP model outlined above are estimated by the maximum likelihood method (Smith, 1989, and Anderson et al., 2001). In order to assess whether the dependence of the location and scale parameters on the time covariates are statistically significant, we use the likelihood ratio test (Coles, 2001).

In the case of the NPP model (non-stationary extreme value analysis) the choice of the threshold is less obvious than in the POT/GPD approach (stationary extreme value analysis), where some experience and empirical rules exist. We will therefore in the non-stationary extreme value analysis use the same threshold defined in the stationary extreme value analysis.

The data sampling follows the usual POT approach, with the peak exceedances and the times at which they occur being represented by  $\{t_{i,j}, x_{i,j}\}$ ,  $j=1, 2, \dots, n_i$ ,  $i=1, 2, \dots, T$ , where  $n_i$  is the number of clusters in the  $i$ -th year. They correspond to the peaks of cluster exceedences

above the threshold  $u$  and the times at which they occur obtained from the 6-hourly timeseries of the hindcast data at MP1. The declustering method we use in order to arrive at this sample is the usual one of identifying clusters and picking their maxima and times where they occur. We have taken care in treating cluster maxima at a distance of less than 48 h apart as belonging to the same cluster (storm) and hence collecting only the highest of the two.

## 5.2 Stationary analysis

In this section we will use the stationary extreme value approach (POT/GPD) to analyse timeseries at MP1 computed with SWAN in non-stationary mode and to define the wind field and wave boundary conditions for a SWAN run in stationary mode.

We start by analysing the 44-year (from 1958 to 2001) wave 6-hourly hindcasts at MP1. These hindcast were computed using the 44-year long ERA-40 dataset and SWAN in non-stationary mode with the settings defined in Section 4 (WAM3 configuration, a directional spreading of  $20^\circ$  and input wind fields increased by 10%, and 1 hour integration time step).

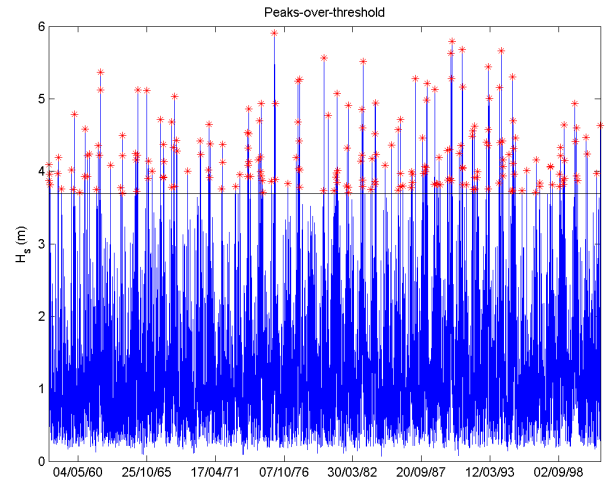


Figure 5.1 Timeseries of  $H_s$  hindcasts at MP1; the red asterisks indicated the peaks selected for the POT sample.

Using the threshold stability property and related tools, we have established that a threshold of 3.7 m was suitable to extract a POT sample from the hindcast timeseries at MP1. The POT sample contained 216 peaks. Figure 5.1 shows the hindcast timeseries and the identified peaks.

We have fitted the GPD distribution to the POT sample, obtaining a scale parameter estimate of 0.68 with a 95% confidence interval of (0.56, 0.82) and a shape parameter estimate of -0.20 with a 95% confidence interval of (-0.32, -0.04). The second estimate indicates that the data

at MP1 come from a distribution with finite support (type III tail) with *endpoint* 7.13 m. This was to be expected since at the MP1 location the wave height is limited by depth. Figure 5.2 shows the return value plot of the data.

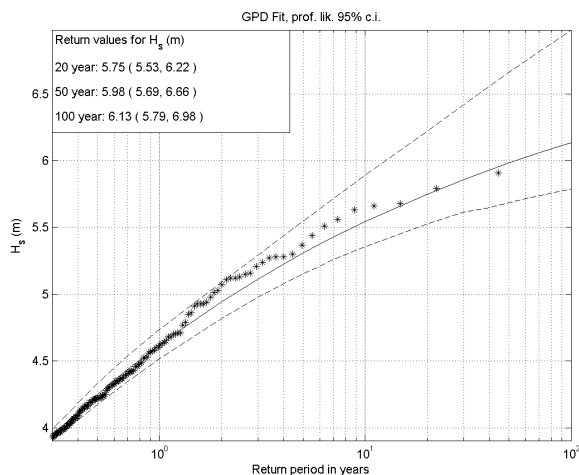


Figure 5.2 Return value plot for the  $H_s$  hindcasts at MP1. The return value estimates are given by the full line, and the respective 95% confidence intervals by the dashed line. The data is given by the asterisks.

The 100-yr return value estimate of  $H_s$  is 6.13 m, with a 95% confidence interval of (5.79, 6.89) m. Using only the  $H_s$ ,  $T_{m02}$  and MWD of the events used in the extreme value analysis, we have determined relationships between  $H_s$  and  $T_{m02}$  and the associated MWD as the direction of the highest events. Using these relationships we estimate the 100-yr values of  $T_{m02}$  and MWD as functions of the 100-yr return value of  $H_s$ ; they are 6.0 s, with 95% confidence interval of (5.8, 6.4) s, and 300°N, respectively. A set of three 100-yr return value estimates obtained in this way will henceforth be called a *100-yr storm estimate*.

In order to compare the 100-yr storm estimate obtained from the 6-hourly hindcasts at MP1 with that resulting from a stationary SWAN approach, we have obtained 100-yr storm estimates at each of the ERA-40 grid points and used them as boundary conditions to force SWAN in stationary mode.

To the timeseries at each ERA-40 grid point we applied the same approach as that used to obtain the 100-yr storm estimate at MP1. Table 5.1 presents the estimates obtained.

We have also analysed the ERA-40 wind speed data and found that at the grid point located at 3°E 54°N the 100-yr return value estimate was of 26.0 m/s with a 95% confidence interval of (24.6, 30.7) m/s. Similar values were obtained at the other ERA-40 grid points at sea.

Using the 100-yr storm estimates of Table 5.1, with the

wind speed being increased by 10% to 28.6 m/s, and setting the directional spreading of the offshore boundary waves at 20°, for consistency with the non-stationary SWAN run, a stationary SWAN hindcast of the storm was obtained. Figure 5.3 shows the computed  $H_s$  field. The associated 100-yr storm estimate at MP1 consists of  $H_s=6.86$ m,  $T_{m02}=6.7$ s and  $MWD=306^\circ$ N.

Location	$H_s$ (m)	$T_{m02}$ (s)	MWD (°N)
3°E 52.5°N	7.95 (7.46, 9.63)	9.8	340
3°E 54°N	10.08 (9.14, 12.84)	10.4	340
4.5°E 52.5°N	7.70 (7.22, 9.35)	10.6	340
4.5°E 54°N	9.64 (8.86, 11.68)	10.4	300
6°E 54°N	9.86 (8.73, 12.80)	10.7	300

Table 5.1 100-yr return value estimates from the ERA-40 data.

Comparing these with those computed from the timeseries hindcast of SWAN in non-stationary mode, we can say that the return value estimate of  $H_s$  from the stationary version of SWAN is higher than the estimate from the non-stationary mode, though still within the 95% uncertainty region of the latter, and that the return value estimate of  $T_{m02}$  from the stationary version even exceeds the endpoint of the 95% confidence interval of the corresponding estimate from the non-stationary mode.

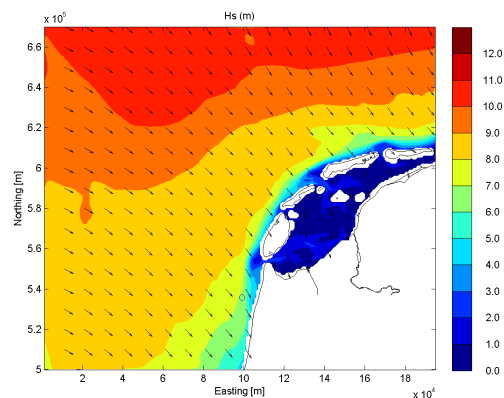


Figure 5.3 100-yr  $H_s$  return values hindcast using SWAN in stationary mode. The MP1 location is marked by a blue circle.

One of the reasons for the discrepancies between the estimates obtained using the stationary and the non-stationary SWAN approach is that the 100 yr return values will not occur at the same time in all the locations of the North Sea region we are considering. For example, the most extreme storm in the ERA-40 data at the west boundary of our grid locations occurred on the 12<sup>th</sup> of December 1990 at 18:00. At those locations the ERA-40  $H_s$  values are close to the estimated 100-yr return value.

This instance, however, does not coincide with the instance when  $H_s$  is highest at the ERA-40 grid point located in the northeast edge of our region, which occurred in 1962. The highest storm hindcast by SWAN in non-stationary mode at the MP1 location occurred on the 3<sup>rd</sup> of January 1976 at 18:00 (the December 1990 storm is the 3<sup>rd</sup> highest storm hindcast at MP1). Figures 5.4 and 5.5 show the  $H_s$  field computed with SWAN in non-stationary mode for the 12/12/1990 18:00 and 3/1/1976 18:00 instances, respectively.

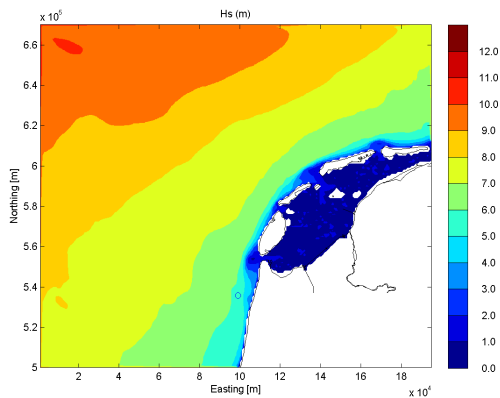


Figure 5.4  $H_s$  values at 12/12/1990 18:00 hindcast using SWAN in non-stationary mode. The MP1 location is marked by a blue circle.

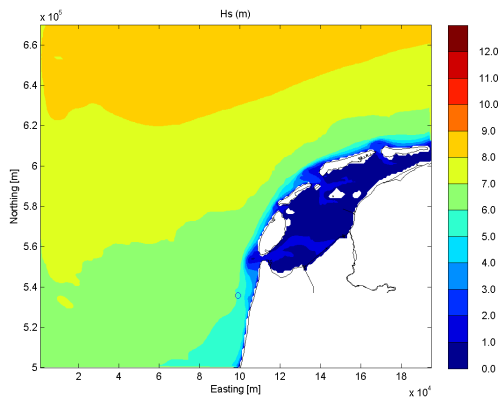


Figure 5.5  $H_s$  values at 3/1/1976 18:00 hindcast using SWAN in non-stationary mode. The MP1 location is marked by a blue circle.

### 5.3 Non-stationary analysis

In order to look for trends or other systematic temporal variations of  $H_s$  in the last decades at MP1, we have analyzed the hindcast timeseries using a non-stationary extreme value approach. We have chosen time ( $t$ ) and its square ( $t^2$ ) as covariates, i.e.,  $P(t)=t$  and  $G(t)=t^2$  in (5.1). Note that the influence of these covariates may be felt in the form of shifts ( $\mu_1$  and/or  $\mu_2 \neq 0$ ) and/or changes in spread ( $\sigma_1$  and/or  $\sigma_2 \neq 0$ ) in the distribution

of extremes, which can be interpreted as increases/decreases in severity and/or variability in extreme wave systems, respectively.

As regards the dependence of the parameters on the covariates, the results of the likelihood ratio tests show that the location parameter is significantly correlated with  $t$  and not with  $t^2$ , and that the scale parameter is not significantly correlated with either  $t$  or  $t^2$ . Thus, time influences the distribution of extremes in the form of shifts (linear trend) but not in the form of changes in spread. The NPP parameter estimates and associated 95% confidence intervals are

$$\mu_0 = 4.46 (4.30, 4.57),$$

$$\mu_1 = 7.4 \cdot 10^{-3} (0.6 \cdot 10^{-3}, 14.5 \cdot 10^{-3}),$$

$$\sigma_0 = 0.49 (0.46, 0.56) \text{ and } \xi = -0.20 (-0.30, -0.06).$$

For the year 2001 the 100-yr return value estimate is of 6.23 with a 95% confidence interval of (5.94, 6.99) m.

Figure 5.6 compares the time dependent NNP 100-yr return value estimate with the estimate obtained from the stationary extreme value analysis.

Thus, according to our NPP analysis there have been significant changes in the extreme value distribution of  $H_s$  at MP1. The changes are in the form of a linear trend of 0.74 cm per year in the location parameter. However, the resulting changes in the 100-yr return value estimates are well within the 95% confidence interval of the estimate obtained from the stationary extreme value analysis.

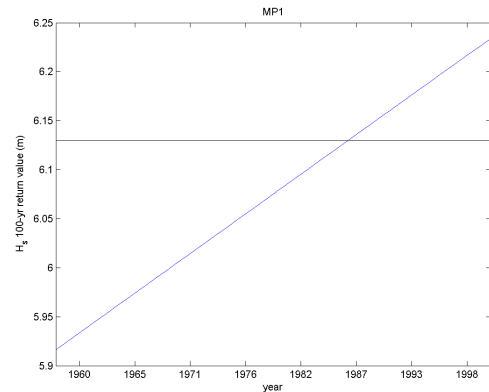


Figure 5.6 Stationary (black line) and non-stationary 100-yr return value estimates (blue line) at MP1 based on the 44-year timeseries of  $H_s$  hindcasts at MP1.

## 6. Conclusions

In this study we have looked at different ways of obtaining return value estimates at nearshore locations. The approaches we have considered were the following:

- 1) Hindcasting extreme storms using SWAN in stationary mode, with stationary extreme value estimates of the boundary conditions and wind fields.
- 2) Hindcasting the nearshore timeseries of wave conditions using SWAN in non-stationary mode with time-dependent boundary conditions and wind fields, and then analyzing the hindcast time series using a stationary extreme value approach.
- 3) Hindcasting the nearshore timeseries as described above, and then analysing the hindcast time series using a non-stationary extreme value approach.

The estimates obtained using approach 1 are conservative when compared with those based on approach 2, both in terms of significant wave height and mean wave period. One of the reasons for the differences in the estimates obtained from approaches 1 and 2 is that the highest storm in so many years does not occur at the same time in all the locations of the North Sea region considered in the boundaries of our study domain. Based on this study we find that, for obtaining return value estimates at nearshore locations, approach 2 is preferable to approach 1.

The estimates based on approach 3 show that in the last 4 decades there has been a small linear increase in severity of the extreme wave systems. The 100-yr return value estimate obtained for the year 2001 using this approach is lower than that based on approach 1 and higher than that based on approach 2, but well within the 95% confidence intervals of the latter.

The estimated linear increase in severity of the extreme wave systems must be interpreted with care. Although it is a long-term trend (44 years) it may still be part of a longer-term cycle or affected by future changes in climate. In order to obtain more consistent future estimates, an approach like that applied by Caires et al. (2006) must be used. Caires et al. (2006) computed future projections of wave systems by using SLP dependent covariates in (6.1). In such a way, once the relation between the present climate extremes and the SLP dependent covariates are established the same relation can be used to compute projections of future extreme wave systems using atmospheric model estimates of SLP fields based on future climate scenarios. There is, however, quite much uncertainty about the scenario to be considered and the atmospheric model used to compute such fields (see Wang et al. 2006).

In the initial stages of this study we have validated the non-stationary SWAN computations and concluded that

- The wind field and wave boundary conditions obtained from the ERA-40 data are suitable for SWAN computations in non-stationary mode.
- The choice of SWAN's integration time step and numerical scheme is not critical. Time steps of 1

hour can be used.

- The choice of the wind input and corresponding whitecapping configuration in SWAN is crucial.
- The hindcasts based on the Westh. configuration describe the high frequency tail of the measured spectra and the measured mean wave periods rather well, but underestimate the wave heights and in particular overestimate the decay of wave energy following the storm peak.
- The best hindcasts are obtained using the WAM3 configuration with properly calibrated input data.

*Acknowledgements.* We thank ECMWF for the ERA-40 data and the Dutch Ministry of Public Works for the North Sea measurements.

## REFERENCES

- Alves, J.H. and M.L. Banner, 2003: Performance of a saturation-based dissipation-rate source term in modelling the fetch-limited evolution of wind waves. *J. Phys. Oceanogr.*, **33**: 1274-1298.
- Booij, N., I.J.G. Haagsma, L.H. Holthuijsen, A.T.M.M. Kieftenburg, R.C. Ris, A.J. van der Westhuysen, and M. Zijlema., 2004: SWAN Cycle III Version 40.41 Users Manual, Delft University of Technology, Delft, The Netherlands, 118 p, <http://fluidmechanics.tudelft.nl/swan/index.htm>.
- Caires, S. and A. Sterl, 2005: 100-year return value estimates for ocean wind speed and significant wave height from the ERA-40 data. *J. Clim.*, **18**, 1032-1048.
- Caires, S., V.R. Swail and X.L. Wang, 2006: Projection and analysis of extreme wave climate. *J. Clim.*, in press.
- Cavaleri, L. and P. Malanotte-Rizzoli, 1981: Wind wave prediction in shallow water: Theory and applications. *J. Geophys. Res.*, **86**, No. C11, 10,961-10,973
- Coles, S., 2001: *An Introduction to Statistical Modelling of Extreme Values*. Springer Texts in Statistics, Springer-Verlag London.
- Eldeberky, Y., 1996: Nonlinear transformation of wave spectra in the nearshore zone, *Ph.D. thesis*, Delft University of Technology, Department of Civil Engineering, The Netherlands
- Hasselmann, K., 1974: On the spectral dissipation of ocean waves due to whitecapping, *Bound.-layer Meteor.*, **6**, 1-2, 107-127
- Hasselmann, S., and K. Hasselmann, 1985: Computations and parameterizations of the nonlinear energy transfer in a gravity-wave spectrum. Part I: A new method for efficient computations of the exact nonlinear transfer integral, *J. Phys. Oceanogr.*, **15**, No. 11, 1369-1377.

- Hasselmann, K., T.P. Barnett, E. Bouws, H. Carlson, D.E. Cartwright, K. Enke, J.A. Ewing, H. Gienapp, D.E. Hasselmann, P. Kruseman, A. Meerburg, P. Müller, D.J. Olbers, K. Richter, W. Sell and H. Walden, 1973: Measurements of wind-wave growth and swell decay during the Joint North Sea Wave Project (JONSWAP), *Dtsch. Hydrogr. Z. Suppl.*, **12**, A8.
- Janssen, P.A.E.M., 1991: Quasi-linear theory of wind-wave generation applied to wave forecasting, *J. Phys. Oceanogr.*, **21**, 1631-1642
- Janssen, P.A.E.M., D. Doyle, J. Bidlot, B. Hansen, L. Isaksen and P. Viterbo, 2002: Impact and feedback of ocean waves on the atmosphere. *Advances in Fluid Mechanics, Atmosphere-Ocean Interactions*, **I**, WIT press, Ed. W. Perrie. 155-197.
- Komen, G.J., S. Hasselmann, and K. Hasselmann, 1984: On the existence of a fully developed windsea spectrum, *J. Phys. Oceanogr.*, **14**, 1271-1285
- Komen, G.J., Cavaleri, L., Donelan, M., Hasselmann, K., Hasselmann, S. and P.A.E.M. Janssen, 1994: *Dynamics and Modelling of Ocean Waves*, Cambridge University Press, 532 p.
- Lalbeharry, R., A. Berhens, H. Guenther and L. Wilson, 2004: An evaluation of wave model performances with linear and nonlinear dissipation source terms in Lake Erie. *Proc. 8th Int. Work. on Wave Hindcasting and Forecasting*, Hawaii, U.S.A.
- Pierson, W.J. and L. Moskowitz, 1964: A proposed spectral form for fully developed wind seas based on the similarity theory of S.A. Kitaigorodskii, *J. Geophys. Res.*, **69**, 24, 5181-5190.
- Ris, R.C., 1997: Spectral Modelling of Wind Waves in Coastal Areas (Ph.D. Dissertation Delft University of Technology), Communications on Hydraulic and Geotechnical Engineering, Report No. 97-4, Delft.
- Ris, R.C., N. Booij and L.H. Holthuijsen, 1999: A third-generation wave model for coastal regions, Part II: Verification, *J. Geophys. Res.*, **104**, C4, 7667–7681.
- Roelvink, J.A., T. van der Kaaij and B.G. Ruesink. (2001). Calibration and verification of large-scale 2D/3D flow models Phase 1. ONL Coast and Sea studies, Project 2: Hydrodynamics and morphology. Report no. Z3029.10. 131 pp.
- Rogers, W.E., P.A. Hwang, D.W. Wang, and J.M. Kaihatu, 2000: Analysis of SWAN model with in situ and remotely sensed data from SandyDuck'97. *Proc. 27<sup>th</sup> Int. Conf. on Coastal Engineering*, Sydney, Australia, ASCE, 812-825.
- Rogers, W.E., P.A. Hwang and D.W. Wang, 2003: Investigation of wave growth and decay in the SWAN model: three regional-scale applications. *J. Phys. Oceanogr.*, **33**: 366-389.
- Smith, R. L., 1989: Extreme value analysis of environmental time series: an application to trend detection in ground level ozone(with discussion). *Statist. Sci.*, **4**, 367-393.
- Toulany, B., W. Perrie, P.C. Smith and B. Yin, 2002: A fine-resolution operational wave model for the NW Atlantic. *Proc. 7th Int. Work. on Wave Hindcasting and Forecasting*, Alberta, Canada, 182-187.
- Van der Westhuysen, A. J., M. Zijlema and J. A. Batjes, 2005: Saturation-based whitecapping dissipation in SWAN for deep and shallow water. Submitted to Coastal Engng.
- Wang, X.L. and V.R. Swail, 2006: Climate change signal and uncertainty in projections of ocean wave height. *J. Climate Dyn.*, **26**, 109-126.
- WAMDI group, 1988: The WAM model - a third generation ocean wave prediction model, *J. Phys. Oceanogr.*, **18**, 1775-1810
- Yan, L., 1987: An improved wind input source term for third generation ocean wave modelling, Sci. Rep. WR 87-8, KNMI, De Bilt, 20 p.
- Yin, B., D. Yang, R. Sha and M. Cheng, 2005: Improvement of different source function expressions in SWAN model for the Bohai Sea, *Progress in Natural Science*, **15**, No. 8, 720-724.